Sensitivity of spaceborne and ground radar comparison results to data analysis methods and constraints

K. Robert Morris, Science Applications International Corporation
Mathew R. Schwaller, NASA Goddard Space Flight Center

35th Conference on Radar Meteorology, American Meteorological Society
Pittsburgh, PA, 26-30 September 2011

ABSTRACT

With the availability of active weather radar observations from space from the Precipitation Radar (PR) on board the Tropical Rainfall Measuring Mission (TRMM) satellite, numerous studies have been performed comparing PR reflectivity and derived rain rates to similar observations from ground-based weather radars (GR). These studies have used a variety of algorithms to compute matching PR and GR volumes for comparison. Most studies have used a fixed 3-dimensional Cartesian grid centered on the ground radar, onto which the PR and GR data are interpolated using a proprietary approach and/or commonly available GR analysis software (e.g., SPRINT, REORDER). Other studies have focused on the intersection of the PR and GR viewing geometries either explicitly or using a hybrid of the fixed grid and PR/GR common fields of view.

For the Dual-Frequency Precipitation Radar (DPR) of the upcoming Global Precipitation Measurement (GPM) mission, a prototype DPR/GR comparison algorithm based on similar TRMM PR data has been developed that defines the common volumes in terms of the geometric intersection of PR and GR rays, where smoothing of the PR and GR data are minimized and no interpolation is performed. The PR and GR volume-averaged reflectivity values of each sample volume are accompanied by descriptive metadata, for attributes including the variability and maximum of the reflectivity within the sample volume, and the fraction of range gates in the sample average having reflectivity values above an adjustable detection threshold (typically taken to be 18 dBZ for the PR). Sample volumes are further characterized by rain type (Stratiform or Convective), proximity to the melting layer, underlying surface (land/water/mixed), and the time difference between the PR and GR observations.

The mean reflectivity differences between the PR and GR can differ between data sets produced by the different analysis methods; and for the GPM prototype, by the type of constraints and categorization applied to the data. In this paper, we will show results comparing the 3-D gridded analysis "black box" approach to the GPM prototype volume-matching approach, using matching TRMM PR and WSR-88D ground radar data. The affects of applying data constraints and data categorizations on the volume-matched data to the results will be shown, and explanations of the differences in terms of data and analysis algorithm characteristics will be presented. Implications of the differences to the determination of PR/DPR calibration differences and use of ground radar data to evaluate the PR and DPR attenuation correction algorithms will be discussed.

P68 SENSITIVITY OF SPACEBORNE AND GROUND RADAR COMPARISON RESULTS TO DATA ANALYSIS METHODS AND CONSTRAINTS

K. Robert Morris*
Science Applications International Corporation / NASA / GSFC
Mathew R. Schwaller – NASA Goddard Space Flight Center

1. INTRODUCTION

Numerous studies have compared reflectivity and derived rain rates from the space-based Precipitation Radar (PR) on board the Tropical Rainfall Measuring Mission (TRMM) satellite to similar observations from ground-based weather radars (GR), using a variety of algorithms to compute matching PR and GR volumes for comparison. Most studies have used a fixed 3-dimensional grid centered on the ground radar (e.g., Schumacher and Houze, 2000; Anagnostou et al., 2001; Liao et al., 2001; Wang and Wolff, 2009), onto which the PR and GR data are interpolated using a proprietary approach and/or commonly available GR analysis software (SPRINT, REORDER). Other studies have focused on the intersection of the PR and GR viewing geometries either explicitly (Bolen and Chandrasekar, 2000), or using a hybrid of the fixed grid and PR/GR common fields of view. For the Dual-Frequency Precipitation Radar (DPR) of the upcoming Global Precipitation Measurement (GPM) mission, a prototype DPR/GR comparison algorithm based on TRMM PR data has been developed that defines the common volumes in terms of the geometric intersection of PR and GR rays, where smoothing of the PR and GR data are minimized and no interpolation is performed (Schwaller and Morris, 2011).

The mean reflectivity differences between the PR and GR can differ between data sets produced by the different volume matching methods; and for the GPM prototype, by the type of constraints and categorization applied to the data. In this paper, we will show results comparing the 3-D gridded analysis "black box" approach to the GPM prototype geometry-matching approach, using matching TRMM PR and WSR-88D ground radar data. The effects of applying data constraints and data categorizations on the volume-matched data to the results, and explanations of the differences in terms of data and analysis algorithm characteristics are presented below. Implications of the differences to the determination of PR/DPR calibration differences and use of ground radar data to evaluate the PR and DPR attenuation correction algorithms are also discussed.

*Corresponding author address: K. Robert Morris, NASA/GSFC Code 422, Greenbelt MD 20771.
E-mail: Kenneth.R.Morris@nasa.gov

2. DATA AND ANALYSIS CHARACTERISTICS

The geometry matching algorithm calculates PR and GR averages at the geometric intersection of the PR rays with the individual GR radar elevation sweeps. The along-ray PR data are averaged only in the vertical, between the top and bottom height of each GR elevation sweep it intersects (Figure 1). GR range bins are horizontally averaged over an area of coverage defined by the half-power points of each PR ray intersected, distance-weighted from the parallax-adjusted center of the PR beam. Each GR elevation sweep is treated separately. The volume-matched data are a set of conical surfaces retaining the vertical coverage defined by the elevation sweeps of the GR volume scan, but with horizontal resolution and location redefined by the PR's scan/ray coordinates. The data gaps between GR sweeps and the "cone of silence" above the highest sweep angle are retained in the geometry-match data set.

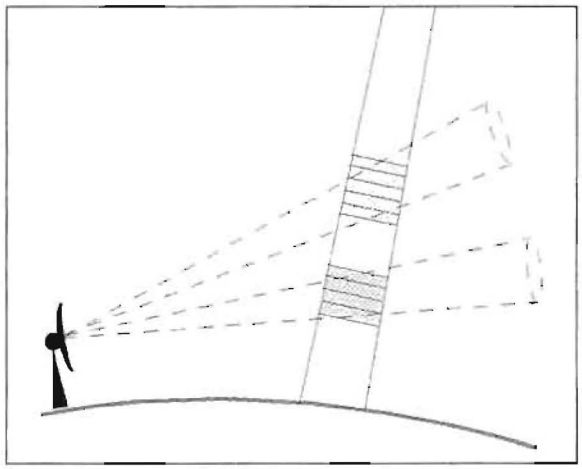

Figure 1. Schematic of PR ray /GR sweep intersections. Shaded areas are "matching volumes" showing the PR gates for one PR ray intersecting GR sweeps (dashed) at two different elevation angles. PR gates are 250 m along-ray by ~5 km in the horizontal.

Unlike the gridded approaches there is no interpolation, extrapolation, or oversampling of data, so matching volumes only exist at somewhat random locations where both the PR and GR instruments have taken actual observations. However, other than for the averaging required to produce the matching volumes, the data are not smoothed; and each sample volume is accompanied by metadata

describing the variability and maximum of the reflectivity within the sample volume, and the fraction of range gates in the PR and GR sample averages having reflectivity values above an adjustable detection threshold (typically taken to be 18 dBZ for the PR). Sample volumes are further characterized by rain type (Stratiform or Convective), proximity to the melting layer, underlying surface (land/water/mixed), and the time difference between the PR and GR observations.

The approaches using analysis of PR and GR data to a fixed 3-dimensional grid centered on the GR treat the PR and GR data separately. While offering the simplicity of a regular coordinate system of fixed location and size, grids represent the scan pattern of neither instrument and thus require some amount of smoothing, interpolation, and extrapolation to attempt to fill as many grid points as possible with data values and fill reasonable gaps in the GR volume scan. All resulting non-missing data points are treated equally, whether or not one or both instruments made observations in the volume represented by the grid box.

In this study, we consider matched PR and GR reflectivity data from the grid-based volume matching algorithm and the geometry-match algorithm. PR data are from the TRMM 2A-25 attenuation-corrected reflectivity product, Version 6. GR data originate from the WSR-88D Level II Archive reflectivity product, which has been quality-controlled to remove non-precipitating echoes (Wolff et al, 2005). Only data samples within 100 km of the ground radar and the overlap of the PR data swath are evaluated. The 3-D grids used are of 4-km horizontal resolution and 1.5-km vertical resolution, with 13 levels centered between 1.5 and 19.5 km height above the GR.

PR data are analyzed to the grid following the methods applied by Liao, et al. (2001). Two different grid analysis methods are applied to the GR data. The first method takes the 2-km-resolution 2A-55 standard TRMM GV product and reduces it to 4 km resolution, as in Liao, et al. (2001). The second method analyzes the Level-II data to the 4-km, 13-level grid using the REORDER radar analysis software. For purposes of comparison to the gridded data, the geometry-match data are grouped into the same 13 vertical levels based on the midpoint height of each sample volume. A mean bright band height is computed for each coincident PR/GR rain case from information provided by the PR bright band detection algorithm, in order to subdivide the data by proximity to the bright band (above, within, or below).

In computing the mean reflectivity differences between the PR and GR, the matched volumes are subdivided into categories based on combinations of the following attributes common to both the grid-based and geometry-match data sets:

- TRMM orbit number (defines date and time of the event)
- GR site identifier
- height layer (13 layers, 1.5-19.5 km)
- proximity to bright band: above, within, or below
- rain type: stratiform, convective, or unknown
- distance from the GR (0-50, 51-100 km)

For each of the data categories defined by the permutations of these attributes, the mean difference between, and standard deviation of, the PR and GR reflectivity for the non-missing sample volumes in the category is computed separately for the grid data and the geometry match data and stored in a data table, along with the identifying attributes and the number of data samples included in the category.

Geometry-match data are subdivided by an additional attribute defined as the fraction of the sample with reflectivity above a minimum instrument detection threshold, defined as 18 dBZ for PR and 15 dBZ for the GR (to match the PR detection threshold but allow for a 3 dBZ calibration difference). The geometry matching algorithm determines, from a pure geometric standpoint, the locations of the PR and GR range bins that are "coincident", and the number of each (number PR expected, number GV expected). Then the reflectivity values of each range gate are evaluated before averaging. The number of PR bins below the 18 dBZ threshold (number PR rejected) and the number of GR bins below 15 dBZ (number GV rejected) are computed and related to each PR and GR sample volume. To compute the PR volume average, the algorithm leaves out those range bins below 18 dBZ and averages the remaining (the same approach is taken in determining the vertically-averaged PR reflectivity for a fixed layer in the grid-based algorithm). No range bins are left out in computing the reflectivity average, maximum, and standard deviation for the GR sample volumes, but those bins below 0.0 dBZ are set to 0.0 dBZ.

From these attributes, a percentage of each sample volume that is above its respective detection threshold is computed for the geometry-match PR and GR. Samples where both the PR and GR percent-above-threshold is non-zero includes all data points with a non-missing reflectivity value, and is akin to the grid-based approach. Restricting the data to samples with a PR and GR percent-above-threshold constraint of 100% provides the best and fairest comparison between the PR and GR instruments, where the entire PR sample volume is above the PR detection threshold, and the entire GR sample volume is filled with echoes above the PR detection threshold. One of the major goals of this study is to show the effects of varying the percent above threshold criteria on the PR-GR mean reflectivity differences. This study computed mean differences from the geometry-matched data for 11 categories of percent-above-threshold cutoff, ranging between 0 and 100%, by 10% steps.

3. SENSITIVITY TO FRACTION OF SAMPLE VOLUME ABOVE DETECTION THRESHOLD

Figures 2-5 show mean PR-GR reflectivity differences for all rainy overpasses at the KMLB (Melbourne, Florida) WSR-88D site from 13 August 2006 to 30 June 2008. KMLB was selected since previous studies have shown it to be closely calibrated to the PR and to have a stable calibration over time (Liao et al., 2001, Liao and Meneghini, 2009a). Figure 2 shows the differences for the convective rain, above bright band category, where the differences based on the geometry-match data have been further subdivided on a sample-by-sample basis by their percent of gates above threshold as described in the previous section. Outside of the percent above threshold, the grid-based results are for the matching categories (orbits, site, rain type, proximity to bright band). Data at height levels above the bright band are merged. Categories where no geometry match samples meet the percent above threshold criteria are eliminated from both the gridded and geometry match data for that percentage, but the gridded data are not otherwise filtered on a sample-by-sample basis.

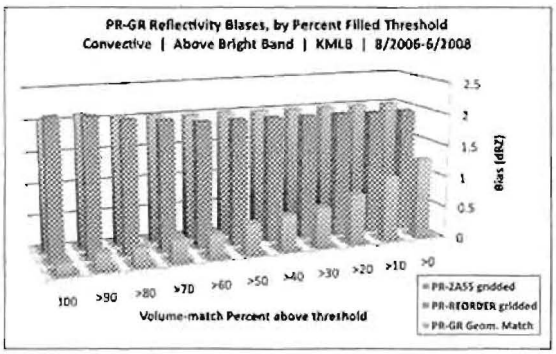

Figure 2. PR-GR reflectivity mean differences at KMLB for convective rain samples above the bright band, by percent above threshold category (see text). PR-2A55 and PR-REORDER series are based on gridded analyses. PR-GR series is from geometry-matched data, using percent above threshold categories from 0 to 100%.

Note the effect of varying the percent above threshold criteria on the PR and GR geometry-match results. As the percent of the sample volume filled with above-detection-threshold reflectivity bins increases, the high bias of the PR to the GR decreases, and vice versa. Much of this is explained by the averaging technique, where only PR bins of 18 dBZ or greater are included in the PR average, while for the GR, all bins are included in the volume average, though the GR percent above threshold measurement for the geometry-matched data is based on the fraction of the GR bins at 15 dBZ or greater. Thus, regardless of the percent above threshold criterion applied to the PR, the lowest PR reflectivity will always be 18 dBZ or greater. The lowest possible geometry-match GR reflectivity included in the mean difference calculation will increase with percent above threshold from just above 0.0 dBZ at percentage values above 0, to 15 dBZ or greater at for samples where 100% of the GR bins in the average are above threshold. The mean differences computed from the gridded data takes all matched PR and GR grid points in the category where the reflectivity values for both are 18 dBZ or greater.

Figure 2 shows that the PR is high biased relative to the GR by about 2 dBZ in the grid-based analyses, and by 1 dBZ or less in the geometry-match analyses. The high bias of the PR relative to the GR in the latter data lowers from 1.26 dBZ to 0.16 dBZ in the geometry-match data as the percent-above-threshold constraint increases from 0 to 100 and the "floor" reflectivity for the GR sample volumes included increases to 15 dBZ, closer to the PR cutoff at 18 dBZ. The grid-based analyses do not change significantly with the change in the percent threshold since the all sample volumes are included for each category. Minor changes occur where grid data for some orbits are excluded when the geometry-match data for the same orbit have no sample volumes meeting the percent-above-threshold criterion of the data category.

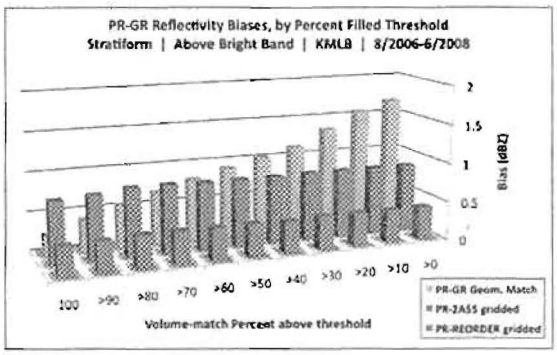

Figure 3. As in Fig. 2, but for stratiform rain type. Order of series is changed from Fig. 2, for visibility.

Figure 3 shows the results for the stratiform rain, above bright band Category. In this case the grid-based PR-GR bias based on the 2A-55 GR product is smaller than the bias based on the REORDER analysis of the GR volume scan, while the geometry match data exhibits the same tendencies but slightly higher PR-GR bias than the convective case. The smaller mean reflectivity differences for the grid-based results compared to the convective case are due to the lower overall reflectivity in the stratiform rain areas, where imposition of an 18 dBZ minimum for the gridpoint sample volumes included in the mean difference calculation puts the grid data in situation approaching the 100% above-threshold constraint applied to the geometry-matched data. There is also likely to be some contamination of the bright band in the grid case, where the bright-band-influenced data are filtered by excluding those fixed layers whose centers lie within 1000 m of the mean bright band.

but, for greater ranges from the radar, the vertical extent of GR bins contributing to such layers may overlap the bright band, raising the GR reflectivity with respect to the PR. The actual top and bottom of each geometry-match sample volume is compared to the mean bright band height when determining whether the sample volume is above, below, or affected by the bright band, so bright band contamination is less likely for these data.

It is this category (stratiform, above bright band) that is used to evaluate calibration differences between the PR and ground radars, as attenuation of the PR at Ku band is at its minimum, and strong horizontal gradients of reflectivity are not present, minimizing the non-uniform beam filling effects. Figure 2 shows that the calibration offset is highly sensitive to the method used to calculate matching PR and GR sample volumes, as well as to the parameters used to select the data samples included in the calculations.

Figures 4 and 5 show the mean differences below the bright band for the convective and stratiform rain rate categories, respectively. The stratiform case in Fig. 5 follows a similar trend to the above-bright-band categories with respect to the change with percent above threshold and the relative biases of the three data sets. The geometry match data for the convective case in Fig. 4 break the pattern of monotonically decreasing PR-GR biases with increasing percent above threshold. In this category, the PR and GR reflectivities change in a similar manner with percent above threshold, perhaps due to the attenuation corrections applied to the PR data.

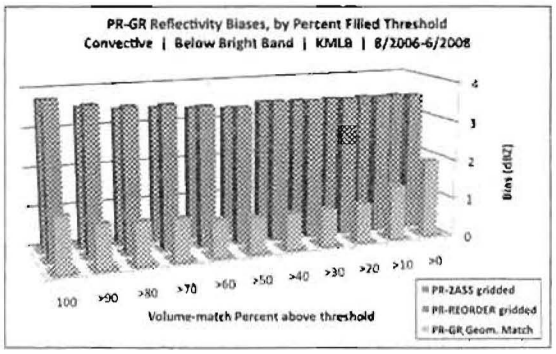

Figure 4. As in Fig. 2, but for convective samples below the bright band.

The overall high bias of the convective samples for the gridded analyses relative to the geometry match data is due primarily to a few cases of very high convective reflectivities. The mean reflectivity differences are weighted by the number of gridpoints in the category, not case-by-case, so a few cases with high PR-GR biases over large areas are driving up the grid-based biases. The difference between the gridded data and geometry match data in these cases is due to the objective analysis scheme used for the PR spreading of the high PR reflectivities over a wider area than they are observed, resulting in high PR reflectivities being differenced against lower GR reflectivities. Since the PR data are averaged only in the vertical in the geometry-match analysis, this source of bias is not present in these data.

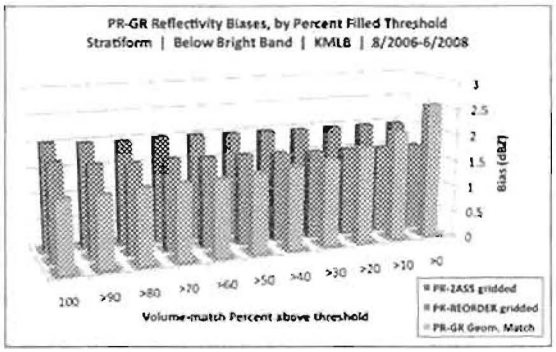

Figure 5. As in Fig. 2, but for stratiform rain samples below the bright band.

4. SENSITIVITY TO PR-GR TIME DIFFERENCES

The time matching rule for PR and GR data selects the GR volume scan with the earliest begin time in a 9-minute window centered on the time of the PR's closest approach to the GR site. The time offset between the PR and GR data has little effect on the mean reflectivity differences, as the mean PR and GR reflectivities do not change significantly in the range of time offsets resulting from this rule. However, the point-to-point reflectivity differences for fast-moving or evolving precipitation echoes should be expected to increase as the time difference increases. To investigate these differences, the standard deviation of the point-to-point differences was computed for each category, and averaged over the full data set. Figure 6 shows these results for the gridded and geometry-match data sets, for the 100% above-threshold category.

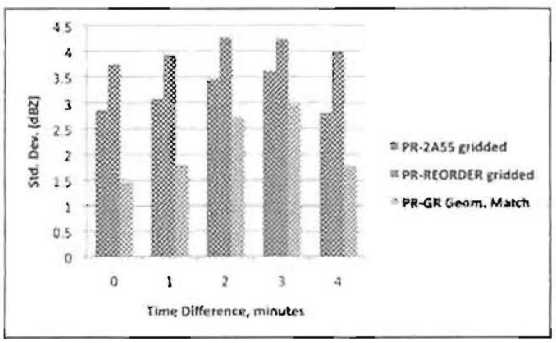

Figure 6. Standard Deviation of PR-KMLB reflectivity differences by time offset between PR and KMLB, for all categories shown in Figs. 2-5, combined.

The standard deviation of the reflectivity differences increases for all 3 data sets as the time difference

between the PR and GR increases from 0 to 3 minutes. The reduction in the standard deviation at 4 minutes time offset is probably a data sampling effect due to the smaller number of data points in this group.

5. SENSITIVITY TO MINIMUM REFLECTIVITY THRESHOLD

By default, the geometry matching algorithm uses a PR threshold of 18 dBZ and a GR threshold of 15 dBZ in determining the fraction of a volume filled with above-threshold reflectivity. The sensitivity of the mean reflectivity differences to changes in these threshold values is demonstrated by changing the GR threshold to 18 dBZ, to match the PR threshold. Table 1 shows mean PR-GR reflectivity differences for the two GR thresholds, split out into stratiform and convective rain regimes both above and below the bright band, limited to those samples 100% filled with above-threshold reflectivity. The data include all cases in years 2008 and 2009 at KMLB. As expected, the PR-GR mean differences for the 18 dBZ GR threshold are lower than for the 15 dBZ threshold, but only by about 0.3 (0.1) dBZ above (below) the bright band, and fewer samples (N) qualify for the higher GR threshold.

Table 1. PR-KMLB mean reflectivity differences (dBZ) for 2008 and 2009 from geometry-match data with GR reflectivity thresholds of 15 dBZ and 18 dBZ. Separate results are shown for convective (C) and stratiform (S) rain, above and below the bright band (BB).

Rain Type / Location	15 dBZ GR threshold		18 dBZ GR threshold	
	mean PR-GR	N	mean PR-GR	N
C / Above BB	0.27	1922	-0.01	1269
C / Below BB	1.03	1154	0.92	1006
S / Above BB	-0.27	2894	-0.63	1566
S / Below BB	2.17	3174	2.10	2382

6. SENSITIVITY TO RANGE FROM GR

Table 2 shows the PR-GR geometry match mean reflectivity differences for KMLB for the data periods used in Figs. 2-6, divided into range categories of 0-50 and 50-100 km from the GR. The sense in which the differences change with distance reverses between stratiform rain, where the differences increase with distance, and convective rain, where the differences decrease with increasing distance. The reason for this difference in behavior is not immediately clear, as both the PR and GR volume averages are affected by the increase in the GR range gate height and width with distance. In either case, away from the bright band the difference between near and far distances is less than 0.4 dBZ for both convective and stratiform rain. The cause of the large differences with distance for the within-bright-band categories needs further investigation, but may be a sampling issue due to the smaller number of samples in the 0-50 km category.

Table 2. PR-KMLB mean reflectivity differences (dBZ) for the geometry match data included in Figs. 2-6, split out by distance from the GR. Separate results are shown for convective (C) and stratiform (S) rain, above, below, and within the bright band (BB).

Rain Type / Location	0-50 km		50-100 km	
	mean PR-GR	N	mean PR-GR	N
C / Above BB	0.30	165	0.14	1182
C / Below BB	1.55	445	1.17	443
C / Within BB	3.04	85	0.37	840
S / Above BB	-0.03	237	0.28	1497
S / Below BB	1.19	1540	1.53	1100
S / Within BB	-2.40	105	-0.66	2818

7. EFFECTS OF S-Ku FREQUENCY MATCHING ADJUSTMENTS

All the comparisons shown up to this point have matched Ku-band PR reflectivity against S-band GR reflectivity, not accounting for expected reflectivity differences due to the different operating frequencies of each instrument. Liao and Meneghini (2009b) provide S- to Ku-band reflectivity corrections for the ice phase (above bright band) and rain phase (below bright band) based on theoretical considerations. Table 3 shows the results obtained comparing the geometry-match unadjusted (S-band) and Ku-adjusted GR reflectivities against the PR, for the same data period as in Table 2 and Figs. 2-6. Note that no correction is attempted for the within-bright-band layer, due to the unknown particle sizes and types in this layer.

Table 3. PR-KMLB mean reflectivity differences (dBZ) for the geometry match data in Table 2, for both unadjusted and frequency-adjusted GR. Separate results are shown for convective (C) and stratiform (S) rain, above and below the bright band (BB).

Rain Type / Location	Unadjusted GR		Ku-adjusted GR	
	mean PR-GR	N	mean PR-GR	N
C / Above BB	0.16	1347	1.35	1347
C / Below BB	1.36	888	-0.30	888
S / Above BB	0.24	1734	0.73	1734
S / Below BB	1.33	2640	0.61	2640

Note that the stratiform rain areas both above and below the melting layer show almost identical PR-GR mean reflectivity differences after the S-to-Ku GR adjustment. The S-to-Ku adjustment relationships are quadratic in terms of Z_e, the reflectivity factor, resulting in larger adjustments to the convective cases. Assuming that the stratiform/above bright band difference represents the residual calibration offset between the PR and GR, then applying this offset to the Ku-adjusted differences shows stratiform differences of 0.1 dBZ or less between PR and GR. A mean PR bias of approximately -1.0 dBZ exists for convective cases below the bright band, indicating an undercorrection for attenuation of the Version 6 PR at low levels in convective rain where PR attenuation is

significant. These results are similar to those computed by Liao and Meneghini (2009b) for KMLB, for post-orbital-boost cases between September 2001 and February 2004.

8. CASE-BY-CASE VARIABILITY

Statistics shown thus far represent averages over all the cases in the time period. For comparison, Table 4 presents mean PR-GR differences on a case-by-case basis (a raining TRMM overpass of the KMLB radar), for the stratiform rain, above bright band category. limited to those points with a percent above threshold of 100%. The results are ordered by the mean value of the maximum PR reflectivity in each remaining non-fixed sub-category (height and distance in this case) and secondarily by orbit number. These data run from August 2006 to June 2008, as in Figs. 2-6. As seen in the results, the mean PR-GR differences for the geometry match data are insensitive to the mean reflectivity, with the exception of two outlier cases for orbits 60537 and 59408. However, the number of samples in the cases tends to increase with the maximum observed reflectivity in stratiform rain.

Table 4. Case-by-case PR-KMLB mean reflectivity differences (dBZ) for stratiform rain, above the bright band. ***PR-2A55*** and ***PR-REORDER*** results are based on gridded PR and GR analyses. ***PR-GR Geo. Match*** results are from geometry-matched data, for the 100% above threshold category.

Orbit #	Mean Max. PR	PR-2A55 gridded		PR-REORDER gridded		PR-GR Geo. Match	
		Mean Diff.	N	Mean Diff.	N	Mean Diff.	N
49886	22	0.76	30	-0.10	18	-0.08	5
56068	22	1.28	23	-0.54	19	0.09	6
54645	23	-0.48	46	-0.72	46	-1.06	10
56248	23	0.16	37	-0.31	32	-0.06	8
49837	23	0.48	149	-0.01	128	-0.27	50
50249	24	-0.08	167	-0.38	140	-0.69	53
56019	24	0.08	40	-0.62	38	-0.70	10
54691	24	0.33	72	-0.07	61	-0.41	40
52676	25	-0.17	5	-0.77	5	1.44	7
50234	25	0.15	27	-0.25	25	-0.15	10
55332	25	0.23	87	-0.37	74	-0.14	56
55668	25	0.34	88	0.03	76	-0.50	43
54752	25	0.64	328	0.30	277	-0.47	132
58751	25	0.79	82	0.51	73	-1.7	19
58049	25	1.14	200	0.61	169	0.09	61
53943	25	3.31	19	3.93	19	0.31	5
50344	26	0.33	20	0.03	16	0.27	6
59136	26	0.37	43	-0.37	39	-1.06	20
56141	26	0.38	390	0.05	318	-0.23	142
50405	27	0.70	502	0.08	412	-0.10	269
59209	27	0.84	83	0.27	77	-0.02	21
60537	27	3.19	158	2.10	152	2.50	164
54908	28	1.55	442	1.13	370	1.06	288
57457	29	0.31	247	0.45	220	0.36	50
54847	30	0.52	314	0.41	285	-0.26	215
59197	30	1.48	117	0.54	99	0.15	44

Table 5 presents the case-by-case results for the convective rain, above bright band category. For this subset of data a pair of strong outlier cases appear for orbits 60537 and 51916 for all three analysis types. It is the large biases and numbers of samples for these cases that contribute to the high values of the PR-GR mean reflectivity differences for convective rain seen in the preceding figures. The reasons for these outlier cases is a subject for further study.

Table 5. As in Table 4, but for convective rain, above the bright band.

Orbit #	Mean Max. PR	PR-2A55 gridded		PR-REORDER gridded		PR-GR Geo. Match	
		Mean Diff.	N	Mean Diff.	N	Mean Diff.	N
49837	27	1.29	15	0.71	14	1.98	5
57457	29	1.84	32	2.08	26	2.73	10
58049	29	1.85	75	1.56	63	0.76	33
50344	30	1.46	39	1	29	1.96	12
56370	32	0.85	42	-0.66	33	-0.59	13
54908	32	1.73	68	1.67	57	1.68	26
54569	35	1.14	16	1.33	15	0.25	8
59209	35	1.54	134	2.35	126	0.08	65
54691	35	1.95	111	1.01	78	0.14	22
56068	36	1.37	23	1	25	2.91	5
56248	36	1.78	54	1.63	43	2.21	16
59957	38	2.71	117	0.91	72	0.28	14
55717	39	1.71	104	1.43	80	-0.39	34
59194	40	0.96	107	2.25	90	-1.06	48
58751	41	1.79	92	2.19	89	0.09	50
59136	42	1.06	83	1.48	60	-1.37	23
50405	42	1.77	394	2.09	316	-0.1	246
54752	42	2.26	164	2.82	140	1.38	78
54847	43	0.83	335	1.51	259	-0.79	251
59148	43	1.5	105	2.09	91	0.65	33
53943	43	1.6	265	2.28	233	-0.95	151
59197	43	2.52	235	2.26	173	-0.55	92
60537	43	5.98	215	5.21	143	3.67	85
51916	44	5.43	53	6.33	50	3.86	27

It is clear from Tables 4 and 5 that the case-by-case variability in the mean reflectivity difference between the PR and GR exceeds that of the effects of sample percent above threshold, minimum GR reflectivity threshold, range from the GR, and S-to-Ku frequency adjustments, and not all of this variation can be ascribed to the size of the data sample in each case.

9. CONCLUSIONS

A new volume-matching algorithm to compare space-based and ground-based radar observations has been developed for the upcoming GPM mission. It allows comparisons to be limited to locations where both systems observe echoes, with no interpolation or extrapolation of the data, and allows the quality of the matching volumes to be controlled in terms of beam filling aspects. The geometry-matched data from this algorithm are compared to traditional grid-based analyses of the same data and are shown to produce a closer comparison between the TRMM PR and the Melbourne, Florida WSR-88D radar.

The two attributes that most affect the geometry-match comparison results are shown to be the percent of the matching volumes filled with reflectivity values above the PR detection threshold of approximately 18 dBZ, and the application of S- to Ku-band frequency adjustments to the ground radar data, each of which can change the long-term mean reflectivity differences by up to 1.5 dBZ. Geometry-match and grid-based comparison results for stratiform rain were similar, however for convective rain the PR was much more high-biased against the GR for gridded analysis when compared to the geometry-match result.

Mean reflectivity differences were relatively insensitive to the time difference between the PR and GR for the range of time differences allowed in the data set, though the scatter of the point-to-point differences is seen to increase with increasing time differences. Mean PR-GR reflectivity differences as a function of distance from the ground radar trended in opposite directions for stratiform and convective rain, with a maximum absolute difference of about 0.4 dBZ for each. The case-by-case variability of the mean reflectivity differences was shown to exceed the variability in the full data set's differences resulting from any of the data analysis, categorization, and frequency adjustment methods applied in the study.

10. RESOURCES

Time-matched TRMM PR and KMLB WSR-88D data files in original formats, geometry match netCDF data files produced from these data, and the Data User's Guide for the geometry match data are freely available for download, as is open source code used to perform the geometry matching and generate displays and statistical comparisons between the PR and GR. Refer to the online links within the *Validation Network Software and Data Products* section of:

http://pmm.nasa.gov/science/ground-validation

11. REFERENCES

Anagnostou, E.N., C.A. Morales, and T. Dinku, 2000: The use of TRMM Precipitation Radar observations in determining ground radar calibration biases. *J. Atmos. Ocean. Tech.*, **18**, 616-628.

Bolen, S.M. and V. Chandrasekar, 2000: Quantitative cross validation of space-based and ground-based radar observations. *J. Appl. Meteor.*, **39**, 2071-2079.

Liao, L., R. Meneghini, and T. Iguichi, 2001: Comparisons of rain rate and reflectivity factor derived from the TRMM Precipitation Radar and the WSR-88D over the Melbourne, Florida, site. *J. Atmos. Ocean. Tech.*, **18**, 1959-1974.

Liao, L., R. Meneghini, 2009a: Validation of TRMM Precipitation Radar through Comparison of Its Multiyear Measurements with Ground-Based Radar. *J. Appl. Meteor. Climatol.*, **48**, 804–817.

Liao, L., R. Meneghini, 2009b: Changes in the TRMM Version-5 and Version-6 Precipitation Radar Products due to Orbit Boost. *J. Meteor. Soc. Japan*, 87A, 93-107

Schwaller, M. R. and K. R. Morris, 2011: A Ground Validation Network for the Global Precipitation Measurement Mission. *J. Atmos. Oceanic Technol.*, **28**, 301–319.

Schumacher, C. and R.A. Houze, 2000: Comparison of Radar Data from the TRMM Satellite and Kwajalein Oceanic Validation Site. *J. Appl. Meteor.*, **39**, 2151–2164.

Wolff, D. B., D. A. Marks, E. Amitai, D. S. Silberstein, B. L. Fisher, A. Tokay, J. Wang, and J. L. Pippitt, 2005: Ground validation for the Tropical Rainfall Measuring Mission. *J. Atmos. Ocean. Tech*, **22**, No. 4, 365-380.

Wang, J., D.B. Wolff, 2009: Comparisons of Reflectivities from the TRMM Precipitation Radar and Ground-Based Radars. J. Atmos. Oceanic Technol., **26**, 857–875.

SENSITIVITY OF SPACEBORNE AND GROUND RADAR COMPARISON RESULTS TO DATA ANALYSIS METHODS AND CONSTRAINTS

K. Robert Morris (SAIC, NASA/GSFC) and Mathew Schwaller (NASA/GSFC)

Q: How does the spaceborne TRMM Precipitation Radar (PR) reflectivity compare to ground radar (GR) measurements?

A: It depends ... on numerous factors.

Geometry-Matching Method and definition of "Percent Above Threshold"

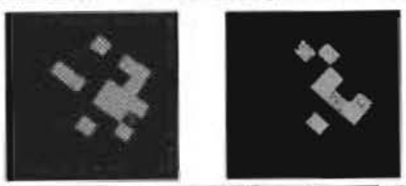

Sensitivity to Percent Above Threshold

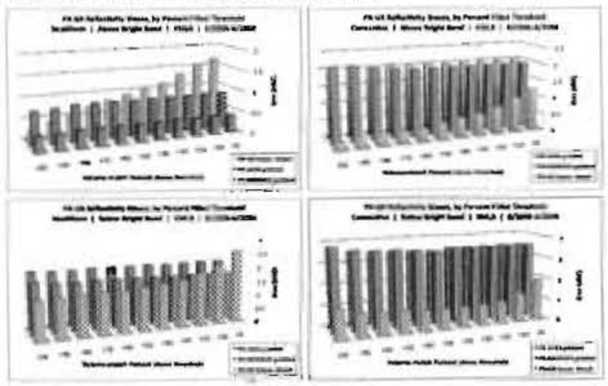

Sensitivity to PR-GR Time Difference

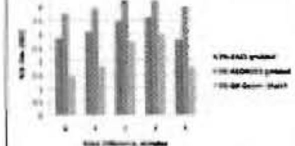

Sensitivity to GR Minimum Reflectivity Threshold

Rain Type / Location	15 dBZ GR threshold		18 dBZ GR threshold	
	mean PR-GR	N	mean PR-GR	N
C / Above BB	0.27	1922	-0.01	1269
C / Below BB	1.03	1154	0.92	1006
S / Above BB	-0.27	2894	-0.63	1566
S / Below BB	2.17	3174	2.10	2382

Sensitivity to Range from the GR

Effects of Radar Frequency Matching

Sample Plots of Geometry-Match and Grid-based Volume Match Data

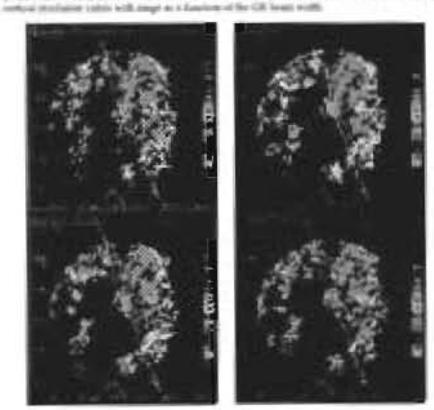

Access TRMM PR and WSR-88D GR data, geometry match data products and documentation, and open source code;

http://pmm.nasa.gov/science/ground-validation

E-mail: kenneth.r.morris@nasa.gov, mathew.r.schwaller@nasa.gov